J Therm Anal Calorim
DOI 10.1007/s10973-017-6304-6

Mild microwave-assisted synthesis of aluminum-pillared bentonites

Thermal behavior and potential applications

Mario D. Ninago[1,3] · Olivia V. López[1] · M. Gabriela Passaretti[1] · M. Fernanda Horst[2] · Verónica L. Lassalle[2] · Irene Carbajal Ramos[3] · Rogelio Di Santo[3] · Andrés E. Ciolino[1,4] · Marcelo A. Villar[1,4]

Received: 21 December 2016 / Accepted: 10 March 2017
© Akadémiai Kiadó, Budapest, Hungary 2017

Abstract Two types of bentonites were modified using a cleaner method to prepare aluminum-pillared clays. This methodology involved a purifying stage, an intercalation process, and a microwave irradiation step at low energy power. Structural changes induced by pillaring process were demonstrated by thermal behavior, as well as morphological characterization. The effect of pillaring process on thermal stability of clays was studied, and the mass lost associated with the dehydroxylation of the octahedral clay sheets was not detected for modified bentonites. In addition, an analysis of their chemical composition and crystalline structure was also performed. Concerning industrial applications of these bentonites, two potential uses were proposed: (1) as reinforcement of different polymers matrices such as thermoplastic starch (TPS), high-density polyethylene (HDPE), and poly (styrene-*b*-butadiene-*b*-styrene), SBS; and (2) as removal agent for cadmium (Cd) species present in wastewaters. Bentonite particles reinforced thermoplastic starch matrix and increased ultraviolet barrier capacity of HDPE composites. Besides, bentonites improved the mechanical performance and modified barrier properties of SBS. Regarding effluents purification, an adequate Cd adsorption from aqueous solutions was observed (77%), proving their feasibility to be used as non-conventional removal agents.

Keywords Aluminum-pillaring · Bentonite · Thermal behavior · Polymeric filler agent · Wastewaters · Cd removal

✉ Mario D. Ninago
mninago@plapiqui.edu.ar

[1] Planta Piloto de Ingeniería Química, PLAPIQUI (UNS-CONICET), Camino ''La Carrindanga'' Km 7, CP: 8000 Bahía Blanca, Buenos Aires, Argentina

[2] Instituto de Química del Sur, INQUISUR (UNS-CONICET), Av. Alem 1253, CP: 8000 Bahía Blanca, Buenos Aires, Argentina

[3] Facultad de Ciencias Aplicadas a la Industria (FCAI), Universidad Nacional de Cuyo (UNCuyo), Bernardo de Irigoyen 375, CP: 5600 San Rafael, Mendoza, Argentina

[4] Departamento de Ingeniería Química, Universidad Nacional del Sur (UNS), Av. Alem 1253, CP: 8000 Bahía Blanca, Buenos Aires, Argentina

Introduction

Scientific and industrial interest in natural clays lies in their worldwide abundance, easiness extraction, and low cost [1]. The large deposits of natural clays located in many countries assured the development of local industries focused not only on the mineral extraction but also on their industrial applications [2–4].

Montmorillonite is the main mineral constituent of bentonites, which are dioctahedral smectites. Bentonites have 2:1 phyllosilicates with a layer structure, consisting of octahedral alumina layers sandwiched between two silica tetrahedral ones [2,–5]. They also contain several other components such as quartz, feldspar, carbonates, and metal oxides [6, 7]. Bentonites have a wide application range mainly due to their colloidal and swelling properties, as well as their high plasticity when they are mixed with small amounts of water [7, 8]. In this sense, bentonites can be used as adsorbents, ion exchangers, wine clarification, and catalysts; as well as reinforcing agents of polymeric matrices due to their eco-friendly character, availability, and reusability [9–14].

In order to extend further applications of bentonites, pillaring process is a commonly used option to modify their

Published online: 21 March 2017

structural, thermal, and surface properties [9, 15, 16]. Scientific literature reports different techniques to prepare pillared clays, and it was found that the characteristics of the final materials strongly depend on the synthesis method employed [17]. The pillaring procedure involves the formation, intercalation, and subsequent fixation of polynuclear cations between clay layers, increasing lamellar spacing and specific area [18]. Modified bentonites are prepared by the insertion of various polyoxocations into clay layers, followed by a thermal treatment [9]. This procedure involves exchange of the interlayer cations with large inorganic polymeric oxy-hydroxy cationic species, spacing the silicate layers and converting layered clay minerals into highly porous structures [17, 18]. Particularly, aluminum-intercalated bentonites are obtained by insertion of Al_{13}-Keggin-like polycations, $[Al_{13}O_4(OH)_{24}(H_2O)_{12}]^{7+}$, between clay layers [19]. Usually, intercalated bentonites are submitted to calcination processes in order to obtain 'pillared' materials, where polyhydroxy cationic species are irreversibly fixed between bentonite layers [2]. In this sense, samples exposition to microwave irradiation at low energy power is a scarcely employed process for replacing mineral clays calcination. This alternative methodology is in accordance with policies dealing with higher awareness regarding environment.

Concerning potential applications of bentonites, clays can act as pollutants scavengers in wastewaters [5, 20] and as fillers of polymeric composites [21, 22], among others. Regarding their use in wastewaters, bentonites play an important role in the environment protection by acting as a natural scavenger of pollutants through an ion exchange process [7]. According to Randelovic et al. [23], several modification methods of mineral clays have been studied nowadays, including physical, chemical, and thermal treatments with the purpose of enhancing their adsorption capacity for certain harmful substances dissolved in water. These minerals have shown a great ability to adsorb a wide variety of heavy metals from water solutions, including Ni(II), Cu(II) [24, 25], Cs(I), Cd(II), Pb(II), U(III) [26], and La(III) [25], among others. Particularly, cadmium (Cd) is a heavy metal that has received special attention regarding its accumulation in sediments, soils, and groundwater [26], and its removal from natural water sources is of great interest [27].

As it was previously mentioned, another important application of bentonites is their incorporation as reinforcing fillers for different polymeric matrices or their use to improve structural, mechanical, and barrier properties of composites. Rohlmann et al. [11] and Magalhães and Andrade [12] stressed that the reason for this interest is mainly related to the potential ability of bentonite particles to be exfoliated into nanometric platelets with high aspect ratio values. Thus, these fillers can well dispersed within the matrices, enhancing final properties of the resulting composites.

The aim of this work was to obtain aluminum-pillared bentonites (Al-pillared) by microwave irradiation, replacing thermal treatments commonly used. Modified bentonites were structurally and thermally characterized, and employed as filler of different polymeric. In addition, their capacity on cadmium removal from wastewaters was also investigated.

Materials and methods

Materials

Natural and commercial bentonites, kindly given by Gabriel Bouillard & Cia (San Rafael, Mendoza, Argentina), were used as starting materials. The commercial bentonite employed in this work is commonly used for clarification processes in wine production. Clays were firstly submitted to a primary crushing in order to reduce material size. Then, samples were sieved in a stack Zonytest (Buenos Aires, Argentina) mechanical sieve shaker, employing standard ASTM sieves N° 40. By using this procedure (in which non-clay material was removed), particles with sizes below 420 μm were obtained. Samples of natural and commercial bentonite were named as M1 and E1, respectively.

Native corn starch was provided by Misky-Arcor (Tucumán, Argentina), and glycerol (Anedra, Argentina) was used as starch plasticizer. High-density polyethylene (HDPE) was supplied by Dow-Polisur S.A., identified as HDPE NG7000 (melt flow index, $MFI = 11$ g 10 min^{-1}, 190 °C/21.6 kg, ASTM12348). Poly(styrene-*b*-butadiene-*b*-styrene) (SBS) was purchased from Sigma-Aldrich ($Mw = 140{,}000$ g mol^{-1} by GPC and 30 mass% styrene).

Purification of bentonites

Samples were subjected to a purification procedure, including the removal of soluble salts and carbonates by successive washes with distilled water and acetate-acetic acid (Cicarelli, Santa Fe, Argentina) buffer solution (pH 4.9), respectively. To solubilize salts, samples were dispersed in distilled water (20 g clay L^{-1} water) and stirred for 24 h at room temperature. Then, suspensions were centrifuged at 1000 rpm for 30 min, and the solid phase was dried at 120 °C. Carbonates removal was performed by adding the buffer solution to clay samples (40 mL buffer g^{-1} clay) and stirring for 12 h at 60 °C. Samples were then recovered by filtration and washed 4 times with distilled water. Before each wash, a centrifugation step at 4500 rpm for 10 min was carried out and the solid phase was recovered and dried at 120 °C.

Preparation of Al-pillared bentonites

First, clays were submitted to a homo-ionization process by stirring the washed samples with 3 M NaOH solution (5 g clay 100 mL^{-1} solution) during 24 h. After this treatment, they were washed with distilled water several times and dried at 120 °C.

Al-pillared agent was prepared following the procedure reported by several authors [2, 28, 29]. A 0.4 M NaOH solution was slowly added dropwise to a 0.4 M $A1C1_3$ solution, at 60 °C, under continuous stirring, by keeping a $[OH^-]/[A1^{3+}]$ equal to 2.2. The resulting solution was aged at 80 °C for 2 h, and for 24 h at room temperature.

Clay aqueous suspensions at 2% (w/v) were prepared, and Al-intercalating solution was slowly added at 60 °C, keeping a relation of 12 mol Al^{+3} g^{-1} clay. Samples were stirred for 2 h at 80 °C and 12 h at room temperature. Intercalated bentonite samples were separated by vacuum filtration and washed with distilled water seven times until the filtrate became free from chlorides, following the procedure reported by Tomul [30]. Solids were separated and dried at 105 °C for 24 h. Dried solids were then sieved in a stack Zonytest mechanical sieve shaker, employing standard ASTM sieve N° 40 (420 μm). Samples of Al-intercalated natural and commercial bentonites were named M2 and E2, respectively.

M2 and E2 samples were submitted to microwave irradiation (Whirlpool, Buenos Aires, Argentina) for 10 min, by employing 100 W power, following the methodology previously described by Olaya et al. [31]. Samples of natural and commercial Al-pillared bentonites subjected to this procedure were named M3 and E3, respectively.

Morphological characterization of bentonites

Bentonites samples were microstructural characterized by scanning electron microscopy (SEM). Samples were dispersed over 3M® aluminum conductive tape sticked onto stubs by using an air flow. Then, they were coated with gold in a sputter coater SPI, and observed in an LEO 40X-VP Scanning Electron Microscope (Jena, Germany), operated at 10 kV. The topographical characteristics of particles were obtained from secondary electron signal. Particles size distribution was studied by laser diffraction (LD) using a Horiba Partica LA-950 Laser Diffraction Particle Size Distribution Analyzer (Kyoto, Japan).

Study of composition and crystalline structure of bentonites

Crystal structure and purity of bentonites were determined by X-ray diffraction (XRD). Diffractograms were obtained in an X-ray diffractometer Philips PW1710 (Almelo, the Netherlands), provided with a tube, a copper anode, and a detector operating at 45 kV and 30 mA within 2θ from 3° to 60°. Besides, according to Bragg's equation, basal spacing or d_{001} reflection of the samples was calculated by monitoring the diffraction angle 2θ from 2° to 10°. After X-ray scanning of the samples, mineral peaks were identified using APD Philips Analytical software. Semi-quantitative analysis was performed by X-Ray Fluorescence Spectroscopy (XRF) using a MagíX Pro XRF spectrometer (Model ARL 8410 (Birmingham, UK) with a Rhodium anode. For this purpose, bentonites were mixed with boric acid in order to obtain compact samples suitable for the analysis. Concentrations of major elements and oxides were determined using IQ + Standardless de PANalytical software.

Thermal analysis of bentonites

This study was carried out in a thermogravimetric balance TA Instrument Discovery Series (New Castle, US). Samples were heated from 30 to 700 °C at 10 °C min^{-1}, under nitrogen flow. Curves of mass percentage as a function of temperature were recorded, and the maximum decomposition temperature was obtained from the first derivative curves (DTG).

Use of bentonites as filler of polymeric composite materials

In an effort to find an alternative application for commercial bentonites, composites based on different polymeric matrices containing E1 were analyzed. The composites preparation and characterization are described in the following paragraphs.

Mixtures of native corn starch, glycerol (30 mass%), distilled water (45 mass%), and E1 (0, 1, 3 and 5 mass%) were prepared. Bentonite was premixed with starch to achieve good particle dispersion between both powders. Then, glycerol and distilled water were added, and samples were mixed and conditioned at 25 °C for 24 h. Conditioned mixtures were melt mixed in a Brabender® Plastograph machine (Duisburg, Germany) at 140 °C and 50 rpm for 15 min, in order to obtain the final composites materials. Films of the processed samples were obtained by thermocompression using a hydraulic press at 150 kg cm^{-2} (140 °C, 6 min). Films homogeneity and appearance were examined by SEM, using the aforementioned microscope. Films were cryo-fractured by immersion in liquid nitrogen, mounted on bronze stubs, and coated with a gold layer ($\sim$30 Å), using an argon plasma metallizer (sputter coater PELCO 91000 (CA, US). Crystal structure identification and degree of bentonite intercalation were studied by XRD, using the aforementioned equipment and conditions.

Degree of crystallinity (C_D) was calculated by Eq. (1) proposed by Soliman and Furuta [32]:

$$C_D\% = \frac{A_c}{A_c + A_a} \times 100 \quad (1)$$

where A_c and A_a correspond to the area of crystalline and amorphous phase, respectively. Mechanical behavior was measured in an Instron 3369 universal machine (Instron, USA) through tensile tests. For stress–strain tests, ten probes of 13 × 100 mm of each film formulation were assayed. Maximum tensile strength (σ_{max}), elongation at break (ε_b) and elastic modulus (E) were calculated according to the ASTM D882-00 (1996). Differential scanning calorimetry (DSC) was performed on a Discovery DSC (TA Intruments, USA). Assays were carried out under nitrogen atmosphere. Approximately, 10 mg of each sample was tested and heated from −100 to 180 °C at 10 °C min^{-1}.

HDPE composites containing E1 (0, 1, 3 and 5 mass%) were prepared by processing in a Brabender® Plastograph machine (Duisburg, Germany) at 160 °C and 40 rpm for 15 min, under nitrogen atmosphere. Films were obtained by thermo-compression using a hydraulic press at 180 kg cm^{-2} (160 °C, 6 min). Films homogeneity and appearance were examined by SEM, by using the aforementioned equipment. Opacity and UV barrier capacity were determined from the absorbance spectra (200–700 nm) recorded in a Shimadzu UV-160 spectrophotometer (Columbia, US). Films were placed on the internal side of a quartz spectrophotometer cell. Film opacity (AU nm) was defined as the area under the recorded curve determined by an integration procedure according to Piermaría et al. [33], and the standard test method for haze and luminous transmittance of transparent plastics recommendations (ASTM D1003-00). Films color measurements were performed using a Hunterlab UltraScan XE (Reston, US) colorimeter in the reflectance mode. Color parameters L, a, and b were recorded according to the Hunter scale, in at least ten randomly selected positions for each film sample. Color parameters range from $L = 0$ (black) to $L = 100$ (white), $-a$ (greenness) to $+a$ (redness), and $-b$ (blueness) to $+b$ (yellowness). DSC analysis was performed using the aforementioned equipment and conditions, heating samples from 40 to 180 °C at 10 °C min^{-1}.

Composites based on SBS and E1, (0 and 5 mass%) were also prepared. First, film samples of SBS were casted from a 25% w/v solution of triblock in isopropylbenzene (cumene) without bentonite, followed by evaporation and drying in a vacuum oven at 60 °C for a week in order to eliminate the remaining solvent. Then, bentonite was added to polymer solution and stirred for 3 h at room temperature to achieve a good dispersion of clay particles. Finally, films were obtained using the same casting procedure as before. Films homogeneity and appearance were examined by SEM, using the same microscope aforementioned. SEM samples were prepared using the technique described for the other polymer matrices. A model 3369 Instron Tensile Testing Instrument (Buckinghamshire, UK) was employed to determine the mechanical behavior of the films. 'Dog-bone' specimens (length: 3 cm, width: 0.4 cm, and thickness: 0.2–0.6 cm) were cut and assayed using a deformation speed of 10 cm min^{-1}. Elastic modulus was calculated according to the ASTM D628-Type V. Oxygen mass transfer rates were analyzed at 25 °C using a Mocon OX-Tran2/20 (Minneapolis, US) based on the ASTM 3985 standard method. Water vapor permeability (WVP) was performed using a PERMATRAN-W Model 3/33 (Minneapolis, US) to measure films water vapor transmission, according to ASTM F 1249-89 standard method. Thermal properties were determined by DSC employing the equipment and conditions previously described, heating samples from −100 to 180 °C at 10 °C min^{-1}.

Use of bentonites for wastewater remediation

Adsorption assays of Cd(II) on bentonite samples were carried out in a batch system by keeping 25 mg of adsorbent in contact with 25 mL of Cd(II) standard solution (100 mg mL^{-1}). Samples were stirred at room temperature and at pH ∼ 6, during 6 h. Then, solutions were centrifuged (5000 rpm) for 30 min and non-adsorbed metal ion concentration in the supernatant was determined by atomic absorption, using a GBC Avanta 932 spectrophotometer (Hampshire, US). The adsorbed percentage of Cd(II) was estimated by the difference between the initial Cd(II) concentration in the original solution and in the resulting supernatant.

Results and discussion

Morphological characterization of bentonites

SEM micrographs (Fig. 1a–c) show the surface morphology of the studied bentonites (M1 and E1). Both minerals showed a typical microstructure clay bentonites (zoom image), conformed by layer slices usually called corn-flake morphologies [34]. Similar internal structures for different clays were reported by Sun et al. [35] and Choo and Bai [1]. M1 and E1 particles showed pores, interstices, and cavities, commonly observed in natural clays, which are related to the high swelling ability of these materials [2, 36–38]. In addition, the presence of pseudo-spherical aggregates with irregular borders is observed.

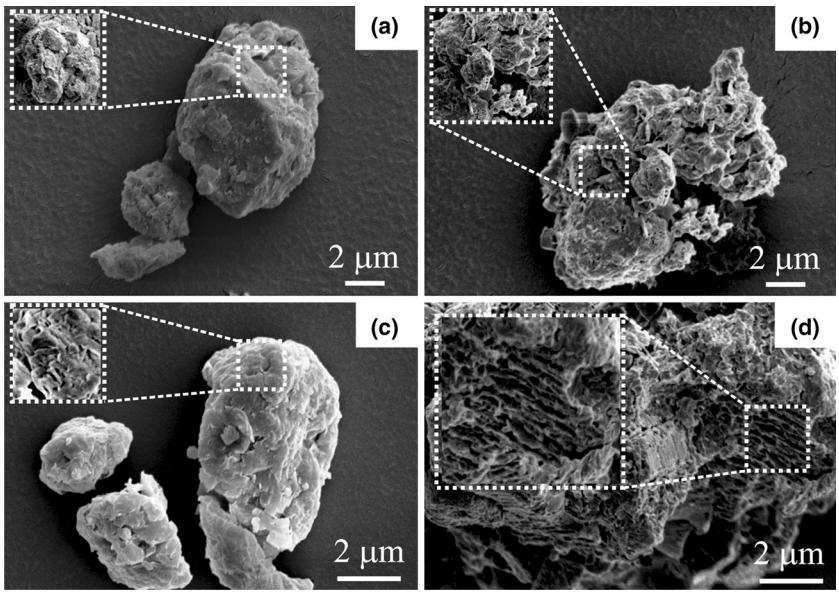

Fig. 1 SEM micrographs of bentonite particles: **a** commercial, E1; **b** Al-pillared commercial, E3; **c** natural, M1 and **d** Al-pillared natural, M3

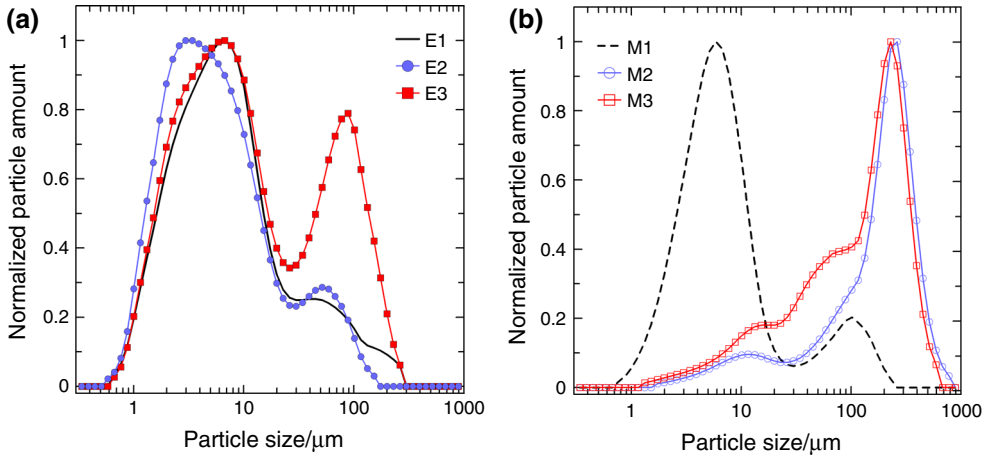

Fig. 2 Size distribution of bentonite particles. **a** Commercial, E1, Al-intercalated commercial, E2, and Al-pillared commercial, E3. **b** Natural, M1, Al-intercalated natural, M2, and Al-pillared natural, M3

Samples were analyzed using different magnifications, and two size particle populations were observed in both clay minerals. Particles agglomeration was observed in E1 samples, with average sizes of ~3.5 and ~13 μm. Concerning to M1, these populations presented sizes of ~5 and ~13 μm (Fig. 1a–c). Modabberi et al. [34] reported similar particle sizes for several Iranian bentonites. Intercalating treatment followed by microwave irradiation led to a less compact structure in both bentonites (Fig. 1b–d). In this sense, E3 and M3 show more spaced crumpled and irregular sheets, giving rise to a mille-feuille structure organization. This appearance was more evident in the case of M3. According to Tomul and Balci [39], the pillaring process by using metallic ions increases particle size and volume. In the case of E3, even though a bimodal particle size distribution was observed, a predominant population of ~84 μm was detected. Concerning M3, these treatments affected the particles size distribution observing mainly aggregates of ~290 μm.

Particle size distributions estimated by laser diffraction (LD) of bulk samples (M1 and E1) are shown in Fig. 2, as well as those of intercalated bentonites (M2 and E2) and the corresponding samples after microwave irradiation treatment (M3 and E3). In the case of E1, a bimodal distribution was distinguished, presenting particles of ~5.8 and ~35.2 μm (Fig. 2a). Equally, natural clay (M1) evidenced two particle size populations with similar values (~5.45 and ~39.8 μm, Fig. 2b).

In both minerals (E1 and M1), the smaller particles represented up to the 90% of the total amount of material. In the particular case of E2 and E3 clays, a bimodal distribution of particles size was observed (Fig. 2a). However, the size of the largest particles resulted significantly higher than the corresponding value obtained for E1, reaching values of

~42 and ~72 μm, for E2 and E3, respectively. In addition, the intercalating process using microwave irradiation led to an increase in the population fraction of bigger particles. In this sense, for E2 this rise was 20% approximately, but for E3 this change was ~40%. For M2, a bimodal particle size distribution was detected (Fig. 2b). Similar to industrial bentonites, intercalating treatment increased significantly the size of both populations of clay minerals, obtaining values of ~184 and ~354 μm. Microwave irradiation modified the particle size distribution of natural bentonites, evidencing three particle populations: ~11, ~121, and ~294 μm (Fig. 2b). Moreover, for M2 and M3 samples the fraction of the bigger particles was 95% of the total amount of measured particles. The effect of pillarization over the size of bentonites agrees well with the discussion reported by Sanabria et al. [40], in which it is stressed that the rise of the particles size could be related to the conformation of pillars between clay layers.

Composition and crystalline structure of bentonites

XRD patterns of all bentonites are shown in Fig. 3. Besides, in this figure is included a table summarizing the main identified crystalline compounds whose concentrations were found higher than 1 mass%. All bentonites were composed basically by montmorillonite (Mt). The reflection of basal plane (001) and the principal reflections of Mt for E1 and M1 were detected at $2\theta = 7.1°$ ($d_{001} \sim 12.4$ Å). These reflections are correctly identified in Fig. 3a–b [41–43]. Besides, in bulk and in the modified bentonites, additional minerals such as quartz and feldspar were also detected. Concerning to feldspar group, hollandite was found in E1 and M1 samples [42]. Regarding to commercial bentonites, the presence of anorthite (other compound of the feldspar group) was observed after the pillarization process [43]. Illite was found in E3 samples [44]. Particularly, for natural bentonites, residues of albite were detected, probably due to the mother rock [44].

XRD analysis revealed that after pillaring, the (001) basal plane (corresponding to Mt) shifted to lower angles for both types of bentonites. Moreover, the interlayer basal spacing (d_{001}) increased significantly, reaching values of 17.6 and 18.6 Å for E3 and M3, respectively. According to Bertella and Pergher [18], this increase in the basal spacing indicates that the clay cations were exchanged for the prepared polyhydroxy cations. The higher increment of

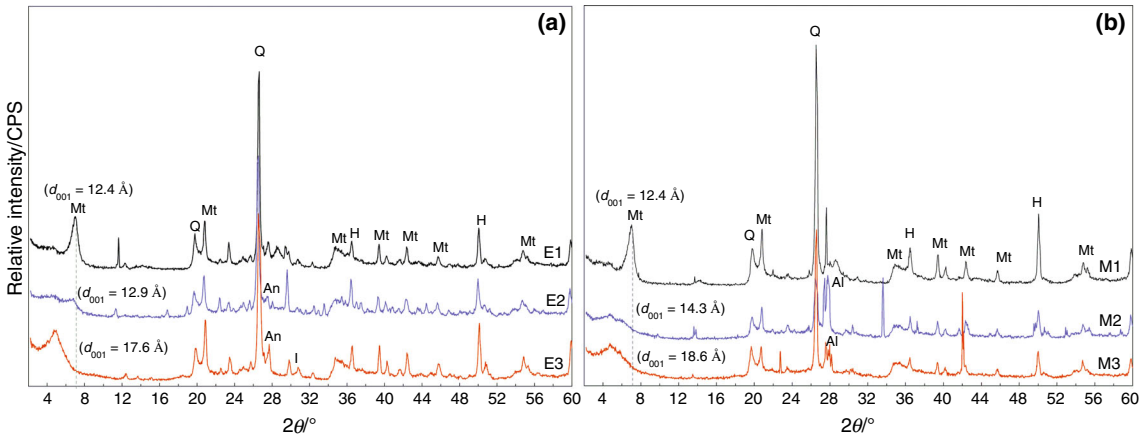

Mineral compound	E1	E2	E3	M1	M2	M3
SiO_2 (Quartz, Q)	✓	✓	✓	✓	✓	✓
$Na_{0.3}(Al, Mg)_2Si_4O_{10}(OH)_2 \cdot xH_2O$ (Montmorillonite, Mt)	✓	✓	✓	✓	✓	✓
$K(Si_3Al)\ O_8$ (Hollandite, H)	✓	✓	✓	✓	✓	✓
(Ca, Na) (Si, Al)$_4O_8$ (Anorthite, An)	x	✓	✓	x	x	x
$Na(AlSi_3O_8)$ (Albite, Al)	x	x	x	x	✓	✓
$K_{0.7}Al_2(Si, Al)_4O_{10}(OH)_2$ (Illite, I)	x	x	✓	x	x	x

✓: Identified compound
x: Non identified compound

Fig. 3 XRD spectra of bentonites. **a** Commercial, E1, Al-intercalated commercial, E2, and Al-pillared commercial, E3. **b** Natural, M1, Al-intercalated natural, M2, and Al-pillared natural, M3. Table summarized the identified crystalline compounds whose concentration was higher than 1 mass%

basal spacing corresponding to M3 is in good agreement with a more intercalated structure of M3 observed by SEM and by LD (Figs. 1–2). These results demonstrated the suitability of using microwave irradiation at low potency to favor clay exfoliation as an alternative to conventional methods such as calcination [18, 20].

Table 1 displays major element contents, determined by X-Ray fluorescence (XRF), of bulk and modified bentonites. In all samples, Si and Al were detected in major proportion in all samples. Concerning to silica, pillaring treatment allowed a slight reduction in its concentration in both bentonites. The pillarization process increased the Al concentration. In this sense, this increment was only ~15% for commercial clays, whereas for natural bentonite this change was significantly more important (~64%). This finding reinforces the aforementioned results obtained by SEM, LD, and XRD techniques.

Thermal analysis of bentonites

TG curves are shown in Fig. 4. The thermal decomposition pattern of E1 presented several differences to those corresponding to modified clays E2 and E3 (Fig. 4a). TG curve of E1 exhibited an initial mass loss step of 5.2%, while for samples E2 and E3 this change was of 10.4 and 9.6%, respectively. This endothermic event, which was extended up to ~110 °C, is characteristic of mineral clays and it is associated to a dehydration process by the removal of water molecules physisorbed in the interlayers (Fig. 4b) [45–47]. The fact that modified commercial bentonites (E2 and E3) evidenced higher percentages of water loss than bulk one (E1) could be associated to the structural changes induced by intercalation and thermal treatments. Moieties of E2 and E3 bentonites could physically adsorb major amount of water molecules than E1, probably due to their higher porosity. This result is in agreement with the less compact structure of E3 compared with E1 observed by SEM (Fig. 1a, b). For the case of modified bentonites, this step also involved the loss of water molecules associated to the Al-oligocations [48, 49]. According to Gil et al. [19], Al-pillared clays undergo several transformation during heating, including the dehydration process of the Al_{13}-Keggin-like polycations, which are metastable polyoxocations that form the stable pillars.

The second thermal decomposition step can be observed at 420 °C for E2 (Fig. 4b). This event could be attributed to desorption of surface hydration water; the loss of structural hydroxyl groups; and a crystal phase change [50]. Finally, for E1 (Fig. 4b), the dehydroxylation of the octahedral clay sheets concluded at around 626 °C. In this aspect, several authors reported similar temperatures values associated with the dehydroxylation of natural and unmodified bentonites [9, 33, 48, 51]. This event was not detected for modified E2 and E3 bentonite samples. Pillars are not simple metal oxides and during heating, cross-linking reactions also take place, involving the formation of covalent bonds between the pillars and clay mineral layers through the hydroxyl groups [19]. These new associations could avoid the dehydroxylation of the clay structure.

Regarding to natural bentonite (M1), TG curve was similar to that corresponding to E1 (Fig. 4c). The first mass loss step of 6.1% can be attributed to the dehydration process. The second degradation step, related to the removal of the more exposed hydroxyl groups of silicate layers, was located at 556 °C. Finally, at 620 °C a last event related to the dehydroxylation of the octahedral clay sheets was detected (Fig. 4d). For modified natural bentonites (M2 and M3), mass losses corresponding to the dehydration process were more pronounced than for M1. These events included the loss of the physisorbed water molecules, as well as those water molecules bounded to the pillars. Similar results were reported by Roca Jalil et al. [49] for aluminum-pillared clays. Modified bentonites M2 and M3 also showed the thermal decomposition step corresponding to the loss of hydroxyl groups associated to the silicate layers. This event was detected at 562 and 572 °C for M2 and M3, respectively (Fig. 4d). In a similar way than modified commercial bentonites, the thermal degradation step related to the dehydroxylation process was not detected for M2 and M3, probably due to hydroxyl groups were compromised by chemical bounds.

Table 1 Chemical composition of the bentonites: commercial, E1; Al-intercalated commercial, E2; Al-pillared commercial, E3; natural, M1; Al-intercalated natural, M2; Al-pillared natural, M3

	Concentration/mass%					
	E1	E2	E3	M1	M2	M3
Si	32.79	28.51	27.79	34.03	27.74	28.02
Al	7.87	9.047	10.43	8.62	14.13	15.52
Fe	1.90	1.58	3.79	1.84	4.074	3.66
Na	1.45	9.601	10.51	1.88	2.00	1.05
K	1.38	1.22	1.89	0.34	0.69	0.60
Mg	0.69	0.65	0.57	1.38	0.822	0.90
Ca	0.56	0.55	0.87	0.34	0.25	0.25

Use of bentonites as filler of polymeric composite materials

SEM micrographs of films based on TPS and TPS/E1-5% are shown in Fig. 5a, b. Fracture surfaces of TPS films resulted homogenous and smooth, without the presence of remnant starch granules. This result could be attributed to the thermal processing effectiveness of these biodegradable materials (Fig. 5a). Additionally, the

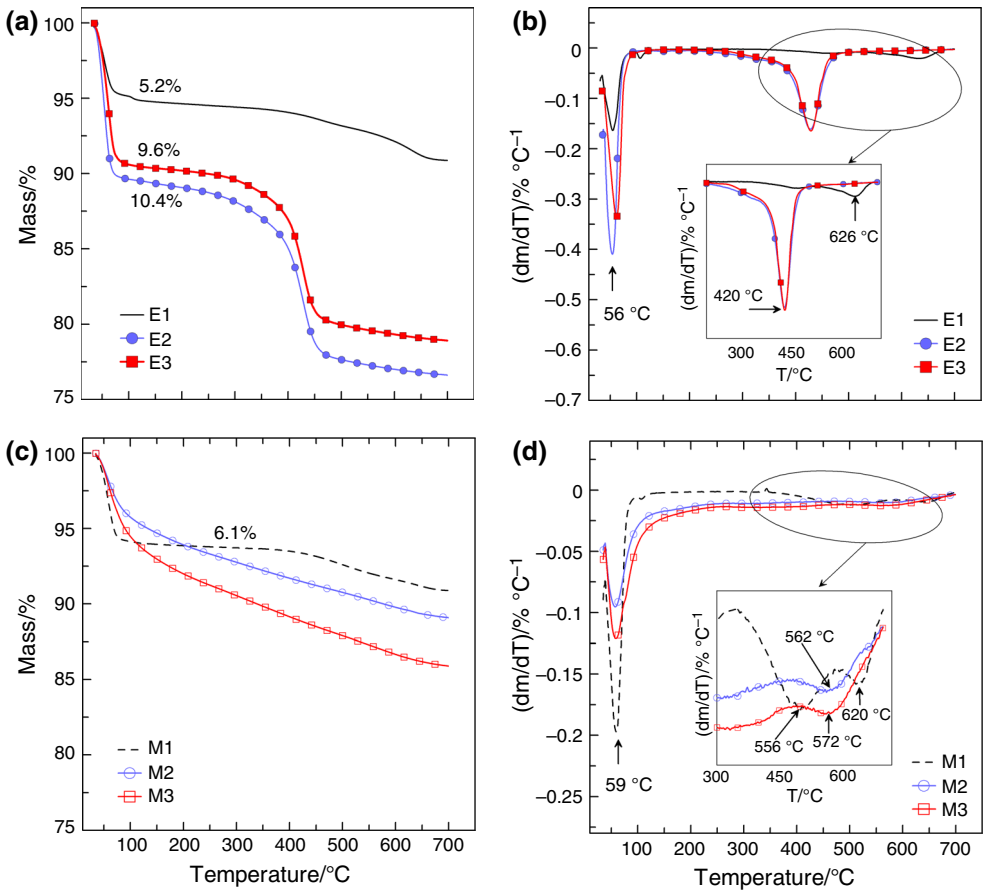

Fig. 4 TG and DTG curves of bentonites. **a**, **b** Commercial, E1, Al-intercalated commercial, E2, and Al-pillared commercial, E3. **c**, **d** Natural, M1, Al-intercalated natural, M2, and Al-pillared natural, M3

phase separation between starch- and glycerol-rich phases was not detected (no channels of plasticizer migration were observed in SEM micrographs). The constant thickness along the films cross section is the result of the efficacy of the thermo-compression process. Concerning to composite films, a good distribution of bentonite particles in TPS matrix was observed (Fig. 5b). This homogeneity in the filler distribution is the consequence of the high efficiency of the melt-mixing process. De Melo et al. [52] reported that composites based on starch and clays presented a continuous fracture surface with a good distribution of the filler within the matrix. The good compatibility between E1 and TPS leads to a good adhesion of the filler to the matrix, avoiding the pulling-out effect of the particles during cryo-fracture of films.

Figure 5c shows the XRD spectra of TPS and E1, as well as those corresponding to TPS/E1-(1–5%) composites. XRD patterns of TPS films were in accordance with a V-type hydrated structure reported in previous works [53, 54].

In order to evaluate the eventual intercalation phenomenon of the TPS between bentonite layers, XRD spectra between $2\theta = 2°$ and 10° were selected because the reflection of (001) plane of bentonites is located in this region. TPS spectrum did not show any reflection in this range, and the peaks detected in XRD spectra of composites at low angles are only attributed to bentonite particles. In Fig. 5c, the (001) plane reflection of E1 in the composite films appeared at lower angles, reaching a displacement of 2.2° for TPS/E1 with 3 and 5 mass% particles. In addition, an increase of ~5.3 Å for interlayer spacing (d_{001}) was observed in the composites with the highest bentonites concentrations (3 and 5 mass%). These results might indicate that TPS chains could be inserted between bentonite layers, conforming intercalated composites. The fact that non-complete exfoliated materials were obtained could be related to the strong polar interactions between hydroxyl groups of the TPS matrix and those presented in the silicate layers [55]. This observation is in accordance with the results reported by Cyras et al. [21] for TPS/montmorillonite nanocomposite films. As a consequence of these interactions, the degree of crystallinity (C_D) of TPS matrix was gradually increased with bentonite concentration (Fig. 5c).

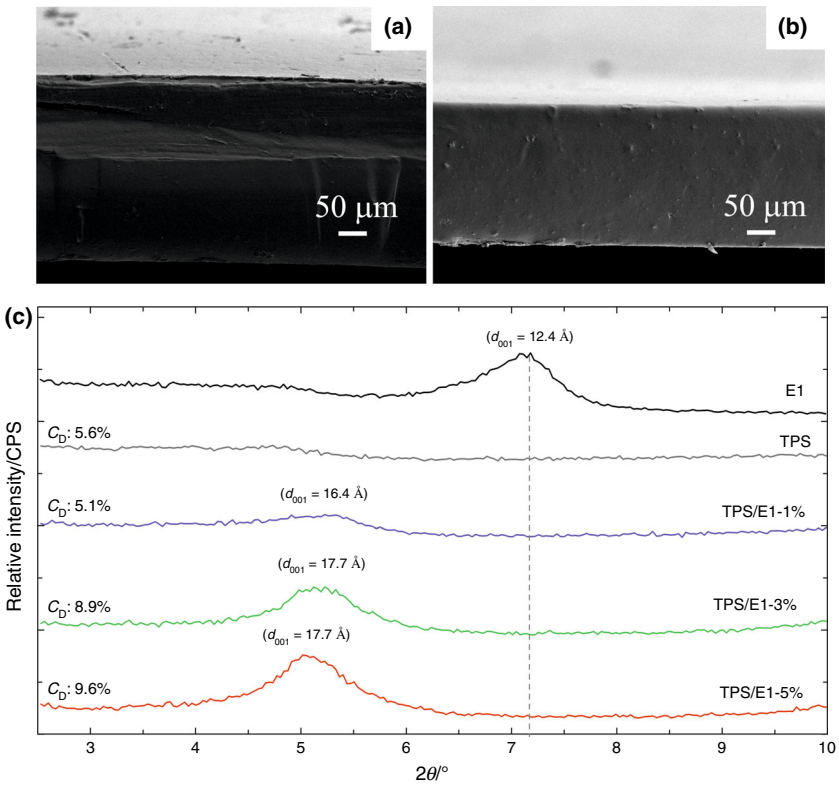

Fig. 5 SEM micrographs of films based on: **a** thermoplastic starch (TPS) and **b** TPS with 5 mass% commercial bentonite, E1. **c** XRD spectra of E1 and TPS with E1 (0, 1, 3, and 5 mass%)

Table 2 Mechanical properties of films based on thermoplastic starch (TPS) with commercial bentonite E1 (0, 1, 3, and 5 mass%)

Film formulation	E/MPa	σ_m/MPa	ε_B/%	Film formulation	L	a	b
TPS	50.9 ± 2.8	1.96 ± 0.36	96.2 ± 8.3	HDPE	88.9 ± 0.2	−0.23 ± 0.02	0.74 ± 0.01
TPS/E1-1%	85.7 ± 7.5	2.45 ± 0.18	87.5 ± 4.2	HDPE/E1-1%	88.4 ± 0.3	−0.19 ± 0.01	0.92 ± 0.09
TPS/E1-3%	94.4 ± 9.0	3.14 ± 0.66	53.1 ± 1.8	HDPE/E1-3%	87.4 ± 0.1	−0.12 ± 0.01	2.39 ± 0.11
TPS/E1-5%	180.9 ± 22.7	3.89 ± 0.15	38.4 ± 6.0	HDPE/E1-5%	84.8 ± 0.7	0.07 ± 0.00	4.04 ± 0.48

Color parameters of films based on high-density polyethylene (HDPE) with commercial bentonite E1 (0, 1, 3, and 5 mass%)

Table 2 summarizes mechanical properties of TPS and TPS/E1 composites obtained from tensile tests. The reinforcing effect of bentonite particles to TPS matrix was evidenced from the increment of both, elastic modulus (E) and maximum tensile stress (σ_m). In this sense, for composites containing 5 mass% bentonite, E and σ_m values resulted 3.5 and 2 times higher than those of TPS matrix. According to Cyras et al. [21], this expected and notorious enhancement in TPS mechanical performance is due to the resistance exerted by the bentonite itself and particles orientation, as well as the aspect ratio of the intercalated layers. These authors also attributed this reinforcement action to the stretching resistance of the TPS chains located into bentonite galleries, because these chains would be bonded by hydrogen interaction to clay layers. However, TPS elongation at break decreased significantly with an increase in bentonite concentration (TPS/E1-5%) because particles exert an obstructive action during tensile test. Other authors had also reported a reduction in TPS films flexibility by mineral particles addition [21, 56]. DSC curves corresponding to TPS and TPS/E1-5% films, as well as tables containing the thermal parameters, are included in Fig. 6. As it can be observed, there are two thermal events: a glass and a melting transition. It is well known that thermoplastic starch materials are constituted by two domains: a plasticized- and a starch-rich phase [54]. The thermal event evidenced at lower temperatures was attributed to the glass transition corresponding to the glycerol-rich phase, giving a glass transition temperature (T_g) of around −65 °C. The addition of E1 bentonite led to a slight increase in the T_g, reaching a value of ~ −61 °C. At higher temperatures, it was found a second event related to the starch melting. Thermal parameters (onset, T_o, and melting, T_m, temperatures, and enthalpy, ΔH) of TPS/E1-

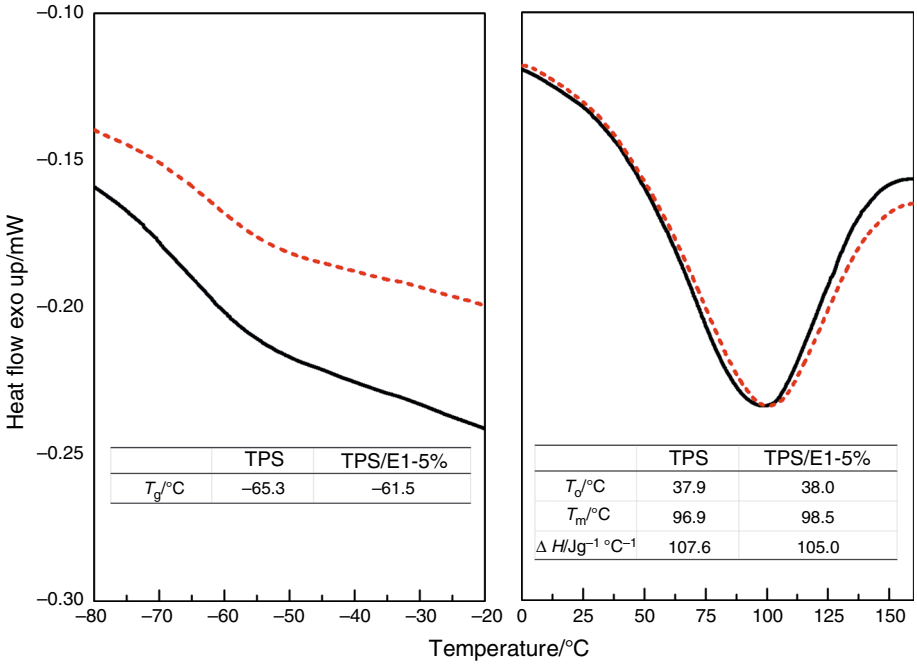

Fig. 6 DSC curves of films based on thermoplastic starch (TPS) and TPS with 5 mass% commercial bentonite, E1. Ref.: —TPS, —TPS/E1-5%

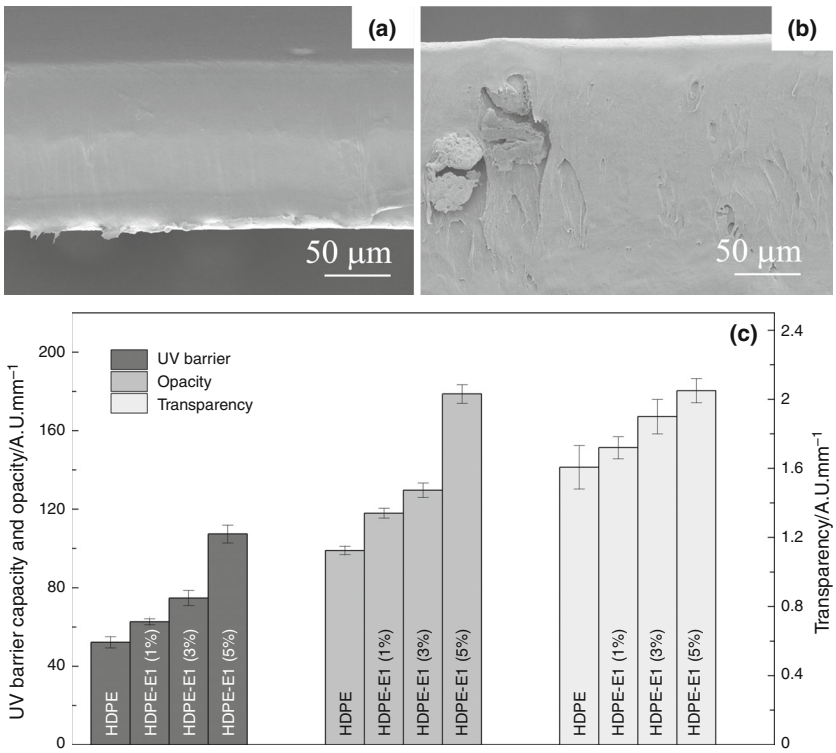

Fig. 7 SEM micrographs of films based on: **a** high-density polyethylene (HDPE) and **b** HDPE with 5 mass% commercial bentonite E1. **c** Optical properties of HDPE with commercial bentonite, E1 (0, 1, 3, and 5 mass%)

5% associated to this transition were not significantly different from those corresponding to TPS films. It is important to highlight that the glass transition of the starch-rich phase was not detected, probably due to the melting endothermic peak could mask this event.

Figure 7 shows SEM micrographs from fracture surfaces of films based on HDPE and HDPE/E1-5%. HDPE showed a smooth and homogeneous cross section (Fig. 7a). Concerning to the composite, even though a good particles distribution within the synthetic matrix was achieved, the presence of several micro-sized bentonite agglomerates was detected (Fig. 7b). Sarifuddin and Ismail [22] found similar morphologies for composites based on poly (ethylene) reinforced with bentonite particles.

Suhaida et al. [57] stressed that irregular shape of bentonites provides a sufficient surface area that enables a good dispersion of the filler by enhancing its fixation to the matrix. Agglomerates formation could be related to the high hydrophilic character of bentonite particles against the hydrophobic one of the synthetic matrix. These agglomerates lead to the particles pulling-out during films cryo-fracture, conducing to the formation of small voids (Fig. 7b). The detachment of bentonite agglomerates indicates a poor interfacial interaction between matrix and the filler [22]. From these results, it is expected that HDPE mechanical performance will be reduced by unmodified bentonite incorporation, because the presence of particle agglomerates could act as stress concentration points [58]. Figure 7c shows the effect of bentonite concentration on optical properties of HDPE films. Particles addition increased UV barrier capacity and opacity of the synthetic matrix. In this regard, the presence of 5 mass% bentonite lead to UV barrier and opacity values of approximately 2 times higher than the corresponding to HDPE films. However, composites resulted less transparent than synthetic matrix, reaching a decrease of 1.3 times in the case of HDPE/E1-5%. These results were attributed to the UV–vis radiation obstruction due to particles blocking effect. Mbey et al. [59] reported a similar effect for composites based on cassava starch and mineral clays. Table 2 summarizes luminosity (L) and color parameters (a, b) of composite films. Regarding to L values, a significant decrease was observed with an increase in bentonite concentration. Particles incorporation at 5 mass% reduced HDPE L values up to ~5%. Concerning to color parameters, a and b values were increased with particles addition, and films became more redness and yellowness. This result might be explained by the inherent color of the bentonite particles used in this study. Figure 8 shows the DSC curves and a table including the thermal parameters of HDPE and HDPE/E1-5% films. As it was expected, a single endothermic transition was detected at around 124 °C, attributed to the polymer melting process. Regarding bentonite incorporation, no significant influence on thermal properties was detected.

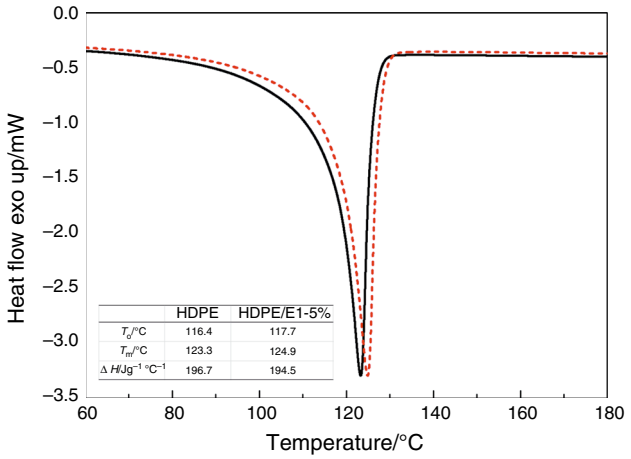

Fig. 8 DSC curves of films based on high-density polyethylene (HDPE) and HDPE with 5 mass% commercial bentonite, E1. Ref.: — HDPE, —HDPE/E1-5%

SEM micrographs of SBS films and composites with 5 mass% E1 are shown in Fig. 9. In addition, a table summarizing their elastic modulus and barrier properties is also included. Different magnifications were performed to evaluate SBS composites, observing in all cases a typical structure of elastomeric matrices. Similar structures were reported by Lietz et al. [60] studying SBS block copolymers reinforced with nanoclays. This character was attributed to the high percentage of polybutadiene (70 mass%) in the SBS employed in this study. Particularly, the cross section irregularity observed for neat SBS was also related to the softness of these matrices (Fig. 9a). The processing technique employed to obtain SBS composite films allowed an adequate bentonite distribution within the matrix. However, the occurrence of some particles aggregates (Fig. 9b) was evidenced, as for the HDPE composites. The weak SBS-E1 compatibility was the responsible of the pulling-out phenomenon occurred during the material cryo-fracture. Thus, micro-voids present in

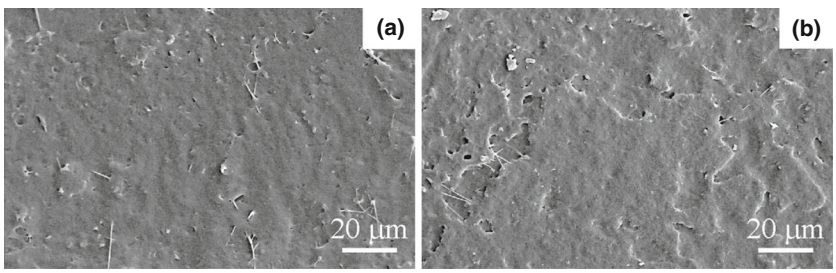

Fig. 9 SEM micrographs of films based on poly(styrene-*b*-butadiene-*b*-styrene) (SBS) and SBS with 5 mass% commercial bentonite, E1.
Table summarizes elastic modulus and barrier properties

Films formulation	Elastic modulus/MPa	Oxygen permeation/cm^3 mil m^{-2} d^{-1}	WVP x 10^{11}/gm^{-1} s^{-1} Pa^{-1}
SBS	14.4 ± 0.8	169.2 ± 6.2	3.14 ± 0.30
SBS/E1-1%	21.5 ± 1.1	136.0 ± 1.6	2.52 ± 0.25

SEM images of SBS/E1-5% could be associated to this poor interfacial adhesion. It is expected that the use of modified clay particles will improve the affinity between the filler and the SBS matrix, reducing this undesirable effect. In this aspect, Liao et al. [61] reported similar results with organophilic montmorillonite clays. Pedroni et al. [62] reported that another alternative to overcome this incompatibility could be processing SBS composites by extrusion instead of casting. These authors suggested that high temperatures and high shear forces present in the thermo-mechanical process can promote physical and chemical interactions between the filler and polymer. Concerning to films mechanical properties, value of elastic modulus was ~1.5 times higher for the composite compared with SBS matrix, being ~14.4 and 21.5 MPa for de SBS and composite. The wide range of elastic modulus of SBS terpolymers reported in the literature demonstrates the high dependence of the mechanical performance of these materials with the SBS molecular weight and the percentage of each block, as well as their morphologies. The significant increment of elastic modulus with the addition of 5 mass% bentonite corroborated the reinforcing effect of the filler despite the use of unmodified bentonite. Furthermore, bentonite addition allowed a notable reduction in barrier properties of SBS matrix. Thus, for both oxygen permeation and WVP values a decrease of ~20% was reached. This effect is attributed to the particles presence, which led to a tortuous pathway for gaseous molecules to move through polymeric matrix, increasing the effective path length for diffusion. SBS composites showed DSC curves typical of this kind of triblock copolymers, as it can be seen in Fig. 10. Thus, two glass transition temperatures were detected corresponding to each polymer block. The glass transition temperature related to the polybutadiene block (T_{gPB}) was located at around −83 °C. Meanwhile, the glass transition temperature of the polystyrene block (T_{gPS}) appeared at ~91 °C. Similar to TPS and HDPE composites, bentonite addition did not modify the T_g values of SBS films.

Use of bentonites for wastewater remediation

Clays are minerals obtained from soils and sediments. Due to their small particle size, large surface area, and unique charge characteristics, they can absorb a wide range and variety of contaminants [63]. Table 3 shows the maximum percentage of Cd(II) adsorption for unmodified bentonites (M1, E1) and pillared clays subjected to microwave treatment (M3, E3). The adsorbents that achieved the highest metal removal capacity were the unmodified particles, reaching ~77.0% for E1 and ~40.0% for M1, related to the available Cd(II) in the initial solution. This great Cd(II)

Table 3 Cd(II) adsorption by bentonites: commercial, E1; Al-pillared commercial, E3; natural, M1; Al-pillared natural, M3

Bentonite samples	Maximum percentage of Cd(II) adsorption
E1	77.0 ± 0.7
E3	64.0 ± 0.6
M1	40.0 ± 0.4
M3	22.0 ± 0.1

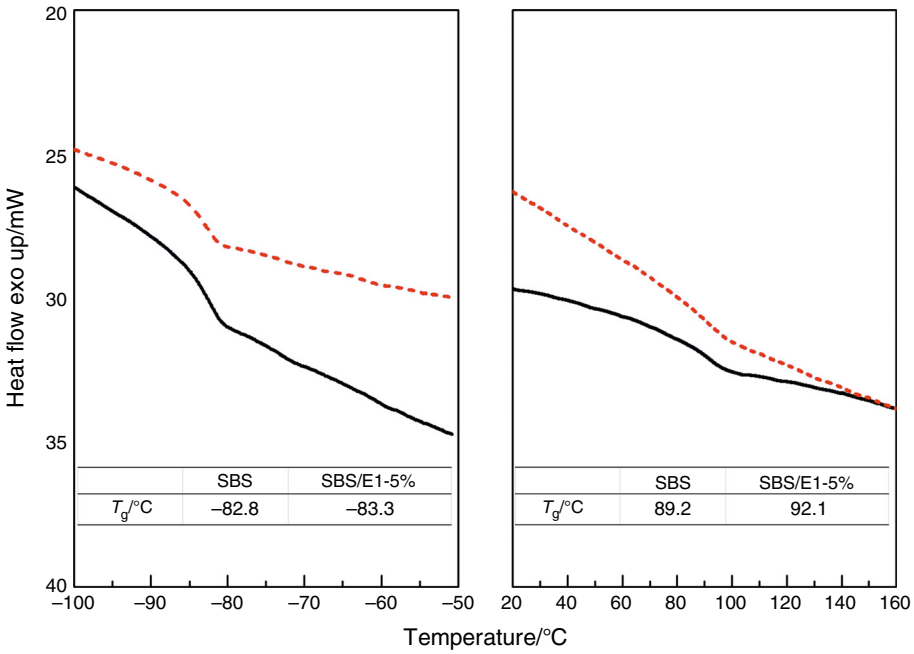

Fig. 10 DSC curves of films based on poly(styrene-*b*-butadiene-*b*-styrene) (SBS) and SBS with 5 mass% commercial bentonite, E1. Ref.: —SBS, — SBS/E1-5%

retention by bentonite samples indicates a high affinity of clays for this metal [20]. In this sense, Schütz et al. [64] demonstrated the efficiency of Cd adsorption by Mn-modified bentonite and bentonite–quartz sand blend. For M3 and E3 samples, a marked reduction in the adsorption capacity of was detected (Table 3). About this, the percentage of cadmium adsorption was ~64.0 and ~22.0% for E3 and M3, respectively. These results are within the range of values reported by Jobstmann and Singh [20]. The lower Cd(II) adsorption observed in pillared compared to natural bentonites was also found by other authors [5, 20]. Jobstmann and Singh [20] stressed that pillared montmorillonite showed smaller Cd adsorption due to its limited adsorptive capacity and low affinity for this metal at pH ~ 6. Additionally, these authors also suggested that the interlayer of the unpillared bentonites adsorbs Cd more effectively than in the pore space of the pillared montmorillonite. The lower Cd retention at shorter period of time by pillared bentonites in relation to unmodified ones could be attributed to a reduction in the clay negative permanent charge, due to the intercalation by a pillaring agent positively charged [5]. In addition, Volzone and Garrido [65] highlighted the relevance of the pH solution over the adsorption capacity of clays. In this sense, Al-pillars exhibited terminal Al–OH^{2+} groups at low pH values. The presence of these species might promote the raise of the electrostatic repulsion between the positively charged groups located at the clay surfaces and the metal ion in the solution.

Conclusions

Commercial (E1) and natural (M1) bentonites were submitted to an intercalation process, followed by microwave irradiation in order to obtain Al-pillared clays. The efficiency of the pillaring process was evidenced studying the analytical composition of clays and their thermal properties. E1 bentonite was employed as filler of TPS, HDPE, and SBS matrices. Particles improved mechanical performance of TPS as consequence of the intercalation of polymer chains between bentonite layers. The addition of bentonite particles modified HDPE optical properties, improving the UV barrier capacity of the composites. Regarding SBS composites, bentonite incorporation enhanced their mechanical and barrier properties. Finally, bentonites presented an adequate Cd(II) adsorption capacity from aqueous solutions, opening the possibility to use them as removal agent for this heavy metal from wastewaters.

Acknowledgements We express our gratitude to the Consejo Nacional de Investigaciones Científicas y Técnicas (CONICET, Argentina, Grant PIP 0428) and the Universidad Nacional del Sur (UNS, Argentina, Grant PGI 24/M135) for their financial support.

References

1. Bertagnolli C, Kleinübing SJ, da Silva MGC. Preparation and characterization of a Brazilian bentonite clay for removal of copper in porous beds. Appl Clay Sci. 2011;53:73–9.
2. Manohar DM, Noeline BF, Anirudhan TS. Adsorption performance of Al-pillared bentonite clay for the removal of cobalt(II) from aqueous phase. Appl Clay Sci. 2006;31:194–206.
3. Alvarez-Ayuso E, Garćia-Sánchez A. Removal of heavy metals from wastewater by natural and Na-exchanged bentonites. Clays Clay Min. 2003;51:475–80.
4. Choo KY, Bai K. Effects of bentonite concentration and solution pH on the rheological properties and long-term stabilities of bentonite suspensions. Appl Clay Sci. 2015;108:182–90.
5. Bergaya F, Lagaly G. Introduction to clay science: techniques and applications. In: Bergaya, F., Lagaly G, editors. Developments in clay science. Handbook of Clay Science; 2013. pp. 1–7.
6. Abu-Jdayil B. Rheology of sodium and calcium bentonite-water dispersions: effect of electrolytes and aging time. Int J Miner Process. 2011;98:208–13.
7. Bhattacharyya KG, Gupta SS. Adsorption of a few heavy metals on natural and modified kaolinite and montmorillonite: a review. Adv Colloid Interface Sci. 2008;140:114–31.
8. Işci S, Günister E, Ece ÖI, Güngör N. The modification of rheologic properties of clays with PVA effect. Mater Lett. 2004;58:1975–8.
9. Caglar B, Cubuk O, Demir E, Coldur F, Catir M, Topcu C, et al. Characterization of AlFe-pillared Unye bentonite: a study of the surface acidity and catalytic property. J Mol. 2015;1089:59–65.
10. Schoonheydt R, Johnston C. Surface and interface chemistry of clay minerals [Internet]. 2nd ed. Handb Clay Sci Elsevier Ltd.; 2006.
11. Rohlmann CO, Horst MF, Quinzani LM, Failla MD. Comparative analysis of nanocomposites based on polypropylene and different montmorillonites. Eur Polym J. 2008;44:2749–60.
12. Magalhães NF, Andrade CT. Calcium bentonite as reinforcing nanofiller for termoplastic starch. J Braz Chem Soc. 2010;21:202–8.
13. Zhou Y, Hu N, Zeng Y, Rusling JF. Heme-protein-clay films: direct electrochemistry and electrochemical catalysis. Langmuir. 2002;18:211–9.
14. Liao R, Bin Yang WY, Chixing Z. Isothermal cold crystallization kinetics of polylactide/nucleating agents. J Appl Polym Sci. 2007;104:310–7.
15. Huang H, Xiao X, Yan B, Yang L. Ammonium removal from aqueous solutions by using natural Chinese (Chende) zeolite as adsorbent. J Hazard Mater. 2010;175:247–52.
16. Yuan P, Annabi-Bergaya F, Tao Q, Fan M, Liu Z, Zhu J, He H, Chen T. TC. A combined study by XRD, FTIR, TG and HRTEM on the structure of delaminated Fe-intercalated/pillared clay. J Colloid Interface Sci. 2008;324:142–9.
17. Katdare SP, Ramaswamy V, Ramaswamy AV. Factors affecting the preparation of alumina pillared montmorillonite employing ultrasonics. Microporous Mesoporous Mater. 2000;37:329–36.
18. Bertella F, Pergher SBC. Pillaring of bentonite clay with Al and Co. Microporous Mesoporous Mater. 2015;201:116–23.

19. Gil A, Korili SA, Trujillano R, Vicente MA. A review on characterization of pillared clays by specific techniques. Appl Clay Sci. 2011;53:97–105.
20. Jobstmann H, Singh B. Cadmium sorption by hydroxy-aluminium interlayered montmorillonite. Water Air Soil Pollut. 2001;131:203–15.
21. Cyras VP, Manfredi LB, Ton-That M-T, Vázquez A. Physical and mechanical properties of thermoplastic starch/montmorillonite nanocomposite films. Carbohydr Polym. 2008;73:55–63.
22. Sarifuddin N, Ismail H. Comparative study on the effect of bentonite or feldspar filled low-density polyethylene/thermoplastic sago starch/kenaf core fiber composites. 2013;8:4238–4257.
23. Ranelovic MS, Purenovic MM, Matovic BZ, Zarubica AR, Momčilovic MZ, Purenovic JM. Structural, textural and adsorption characteristics of bentonite-based composite. Microporous Mesoporous Mater. 2014;195:67–74.
24. Erdem B, Ozcan A, Gök O, Ozcan AS. Immobilization of 2,2′-dipyridyl onto bentonite and its adsorption behavior of copper(II) ions. J Hazard Mater. 2009;163:418–26.
25. Yang S, Li J, Lu Y, Chen Y, Wang X. Sorption of Ni(II) on GMZ bentonite: effects of pH, ionic strength, foreign ions, humic acid and temperature. Appl Radiat Isot. 2009;67:1600–8.
26. Fernández-Nava Y, Ulmanu M, Anger I, Marañón E, Castrillón L. Use of granular bentonite in the removal of mercury(II), cadmium (II) and lead(II) from aqueous solutions. Water Air Soil Pollut. 2010;215:239–49.
27. Ding SL, Sun YZ, Yang CN, Xu BH. Removal of copper from aqueous solutions by bentonites and the factors affecting it. Min Sci Technol. 2009;19:489–92.
28. Morante JA, Pesquera C, Blanco C, González F. Textural characterization of montmorillonite pillared with aluminum/lanthanum polyoxycations. Stud Surf Sci Catal. 2002;144;617–24.
29. Zhang X, Wang Q, Jiang H. research on the preparation of the environmental friendly pillared bentonite and its catalytic properties. In: 2nd international conference on electronic and mechanical engineering and information technology (EMEIT-2012), 2012;959–962.
30. Tomul F. Effect of ultrasound on the structural and textural properties of copper-impregnated cerium-modified zirconium-pillared bentonite. Appl Surf Sci. 2011;258:1836–48.
31. Olaya A, Blanco G, Bernal S, Moreno S, Molina R. Synthesis of pillared clays with Al–Fe and Al–Fe–Ce starting from concentrated suspensions of clay using microwaves or ultrasound, and their catalytic activity in the phenol oxidation reaction. Appl Catal B Environ. 2009;93:56–65.
32. Soliman EA, Furuta M. Influence of phase behavior and miscibility on mechanical, thermal and micro-structure of soluble starch-gelatin thermoplastic biodegradable blend films. Food Nutr Sci. 2014;5:1040–55.
33. Piermaría J, Bosch A, Pinotti A, Yantorno O, García MA, Abraham A. Kefiran films plasticized with sugars and polyols: water vapor barrier and mechanical properties in relation to their microstructure analyzed by ATR/FT-IR spectroscopy. Food Hydrocoll. 2011;25:1261–9.
34. Modabberi S, Namayandeh A, López-Galindo A, Viseras C, Setti M, Ranjbaran M. Characterization of Iranian bentonites to be used as pharmaceutical materials. Appl Clay Sci. 2015;116–117:193–201.
35. Sun Z, Qu X, Wang G, Zheng S, Frost RL. Removal characteristics of ammonium nitrogen from wastewater by modified Ca-bentonites. Appl Clay Sci. 2015;107:46–51.
36. Naswir M, Arita S, Marsi, Salni. Characterization of bentonite by XRD and SEM-EDS and use to increase PH and color removal, Fe and organic substances in peat water. J Clean Energy Technol. 2013;1:313–7.
37. Pramanik S, Das G, Karak N. Facile preparation of polyaniline nanofibers modified bentonite nanohybrid for gas sensor application. RSC Adv. 2013;3:4574–45981.
38. Ding M, Zuo S, Qi C. Preparation and characterization of novel composite AlCr-pillared clays and preliminary investigation for benzene adsorption. Appl Clay Sci. 2015;115:9–16.
39. Tomul F, Balci S. Characterization of Al, Cr-pillared clays and CO oxidation. Appl Clay. 2009;43:13–20.
40. Sanabria N, Álvarez A, Molina R, Moreno S. Synthesis of pillared bentonite starting from the Al–Fe polymeric precursor in solid state, and its catalytic evaluation in the phenol oxidation reaction. Catal Today. 2008;133–135:530–3.
41. Andrini L, Toja RM, Gauna MR, Conconi MS, Requejo FG, Rendtorff NM. Extended and local structural characterization of a natural and 800 °C fired Na-montmorillonite–Patagonian bentonite by XRD and Al/Si XANES. Appl Clay Sci. 2017;137:233–40.
42. Chen J, Li J, Qiying L, Xiumin H, Wenjie S. Facile synthesis of Ag-hollandite nanofibers and their catalytic activity for ethanol selective oxidation. Chin J Catal. 2007;28(12):1034–6.
43. Mahmoudi S, Bennour A, Meguebli A, Srasra E, Zargouni F. Characterization and traditional ceramic application of clays from the Douiret region in South Tunisia. Appl Clay Sci. 2016;127–128:78–87.
44. Sakizci M, Burcu EA, Ertuğrul Y. Thermal behavior and immersion heats of selected clays from Turkey. J. Therm Anal Calorim. 2009;98:429–36.
45. Ursu AV, Jinescu G, Gros F, Nistor ID, Miron ND, Lisa G, Silion M, Djelveh G, Azzouz A. Thermal and chemical stability of Romanian bentonite. J Therm Anal Calorim. 2011;106:965–71.
46. Tomul F. Adsorption and catalytic properties of Fe/Cr-pillared bentonites. Chem Eng J. 2012;185–186:380–90.
47. Tomul F. Influence of synthesis conditions on the physicochemical properties and catalytic activity of Fe/Cr-pillared bentonites. J Nanomater. 2012;2012:3.
48. Bahranowski K, Włodarczyk W, Wisła-Walsh E, Gaweł A, Matusik J, Klimek A, et al. [Ti, Zr]-pillared montmorillonite—a new quality with respect to Ti- and Zr-pillared clays. Microporous Mesoporous Mater. 2015;202:155–64.
49. Roca Jalil ME, Vieira RS, Azevedo D, Baschini M, Sapag K. Improvement in the adsorption of thiabendazole by using aluminum pillared clays. Appl Clay Sci. 2013;71:55–63.
50. Ouellet-Plamondon C, Lynch RJ, Al-Tabbaa A. Comparison between granular pillared, organo- and inorgano-organo-bentonites for hydrocarbon and metal ion adsorption. Appl Clay Sci. 2012;67–68:91–8.
51. Bayram H, Önal M, Yılmaz H, Sarıkaya Y. Thermal analysis of a white calcium bentonite. J Therm Anal Calorim. 2011;101:873–9.
52. de Melo C, Salomao GP, Eiras GM, Yamashita F, Dall'Antonia L, Mali S. Properties of extruded xanthan-starch-clay nanocomposites films. Braz Arch Biol Technol. 2011;54:1223–333.
53. Castillo L, López O, López C, Zaritzky N, García MA, Barbosa S, et al. Thermoplastic starch films reinforced with talc nanoparticles. Carbohydr Polym. 2013;95:664–74.
54. Ninago MD, López OV, Lencina MMS, García MA, Andreucetti NA, Ciolino AE, et al. Enhancement of thermoplastic starch final properties by blending with poly(ε-caprolactone). Carbohydr Polym. 2015;134:205–12.
55. Park H-M, Lee S-R, Chowdhury SR, Kang T-K, Kim H-K, Park SH, Chang SH. Tensile properties, morphology, and biodegradability of blends of starch with various thermoplastics. J Appl Polym Sci. 2002;86:2907–15.
56. Huang M-F, Yu J-G, Ma X-F. Studies on the properties of Montmorillonite-reinforced thermoplastic starch composites. Polymer. 2004;45:7017–23.

57. Suhaida SI, Ismail H, Palaniandy S. Study of the effect of different shapes of ultrafine silica as fillers in natural rubber compounds. Polym Test. 2011;30:251–9.
58. Ismail H, Mathialagan M. Comparative study on the effect of partial replacement of silica or calcium carbonate by bentonite on the properties of EPDM composites. Polym Test. 2012;31:199–208.
59. Mbey JA, Hoppe S, Thomas F. Cassava starch–kaolinite composite film. Effect of clay content and clay modification on film properties. Carbohydr Polym. 2012;88:213–22.
60. Lietz S, Yang JL, Bosch E, Sandler JKW, Zhang Z, Altstädt V. Improvement of the mechanical properties and creep resistance of SBS block copolymers by nanoclay fillers. Macromol Mater Eng. 2007;292:23–32.
61. Liao M, Zhu J, Xu H, Li Y, Shan W. Preparation and structure and mechanical properties of poly(styrene-b-butadiene)/clay nanocomposites. J Appl Polym Sci. 2004;92:3430–4.
62. Pedroni LG, Araujo JR, Felisberti MI, Nogueira AF. Nanocomposites based on MWCNT and styrene-butadiene-styrene block copolymers: effect of the preparation method on dispersion and polymer-filler interactions. Compos Sci Technol. 2012;72:1487–92.
63. Huang W, Chen J, He F, Tang J, Li D, Zhu Y, et al. Effective phosphate adsorption by Zr/Al-pillared montmorillonite: insight into equilibrium, kinetics and thermodynamics. Appl Clay Sci. 2015;104:252–60.
64. Schütz T, Dolinská S, Hudec P, Mockovčiaková A, Znamenáčková I. Cadmium adsorption on manganese modified bentonite and bentonite–quartz sand blend. Int J Miner Process. 2016;150:32–8.
65. Volzone C, Beatriz GL. Use of modified hydroxy-aluminum bentonites for chromium(III) removal from solutions. J Environ Manag. 2008;88:1640–8.